# EFFECT OF FABRIC WEBS ON THE STATIC RESPONSE OF SPINDLE-SHAPED TENSAIRITY COLUMNS

**Thomas E. Wever [1]; Theofanis S. Plagianakos [2]; Rolf H. Luchsinger [3]; and Peter Marti [4], F.ASCE**

**Abstract**

Tensairity is a lightweight structural concept comprising struts and cables stabilized by a textile membrane, which is inflated by low pressurized air. This paper addresses the effect of fabric webs inside the membrane hull on the static response of spindle-shaped Tensairity columns to axial compression. Two full-scale spindle-shaped columns, one without and one with webs, were fabricated and tested. The columns were subjected to axial compressive loading for various levels of internal air pressure in order to quantify its effect on the global structural response. It was found that the stiffness and the load bearing capacity for both columns increased with increasing air pressure. The experimental results also revealed the benefits of including fabric webs in the spindle configuration in terms of axial stiffness and buckling load. Comparisons with an analytical solution and finite element predictions showed good correlation for the axial stiffness in the case without webs. For the case with webs deviations between predicted and experimental results indicated that structural detailing and imperfections in the manufacturing process strongly influence the performance of Tensairity columns with internal webs.

[1] Graduate Student, Faculty of Civil Engineering and Geosciences, Delft University of Technology, Netherlands. E-mail: tomwever@yahoo.com

[2] Post-doctoral Research Associate, Center for Synergetic Structures, Empa, Swiss Federal Laboratories for Materials Testing and Research, Überlandstrasse 129, CH-8600, Dübendorf, Switzerland. E-mail: theofanis.plagianakos@empa.ch

[3] Head of Center, Center for Synergetic Structures, Empa, Swiss Federal Laboratories for Materials Testing and Research, Überlandstrasse 129, CH-8600, Dübendorf, Switzerland. E-mail: rolf.luchsinger@empa.ch

[4] Professor, Institute of Structural Engineering, ETH, Wolfgang-Pauli-Strasse 15, CH-8093, Zurich, Switzerland. E-mail: marti@ibk.baug.ethz.ch

**Subject headings:** Tensairity; Lightweight structures; Inflatable structures; Fabrics; Axial compression; Full-scale tests; Webs.

## Introduction

Inflatable textile structures made up of plain-woven fabrics (polyester, glass, aramide or carbon fibers coated by PVC, silicon, rubber or Teflon) combine very low weight with low storage volume, ease to deploy and enhanced damping capabilities. Inflated textile beams (airbeams) can be utilized in a variety of forms to achieve a high level of aesthetics and a free-form design concept. Moreover, tailoring of their static and damped dynamic response via internal air pressure enables the design of adaptive structural components. Thus, airbeams combine interesting features which could be exploited in several lightweight structural applications.

However, inflated structures and especially airbeams have a relatively poor load bearing capacity. Their small bending stiffness and their inability to carry compressive loads lead to instabilities such as local wrinkling and global buckling. Thus, airbeams have to be inflated to high pressure levels in order to achieve axial and bending stiffnesses comparable to those of conventional structures. The Tensairity® structural concept (Luchsinger et al. 2004) drastically improves the load bearing capacity of an airbeam by combining low pressurized air with cables, struts and a membrane hull (Fig. 1). The applicability of the concept in real bridges and roofs has been demonstrated (Luchsinger and Crettol 2006). Thus, the Tensairity concept combines the advantages of conventional airbeams with a marked improvement of the load bearing capacity and offers a promising potential for temporary structural applications.

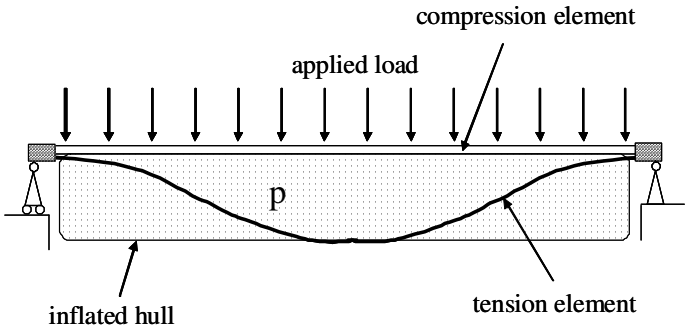


**Figure 1** Structural principle of a Tensairity beam subjected to bending

Substantial analytical and experimental work has been conducted in the area of inflated membrane structures in the last decades. Woven fabrics were first implemented in architectural applications in the late

1940's by Bird (1967), who developed several pneumatic domes (the so-called "radomes"), and in the early 1960's by Otto and Trostel (1962). Extended reviews of inflated membrane applications were made by Bulson (1973), Herzog (1976) and Bernasconi and Reibaldi (1986), whereas fabrication and construction details were described by Sobek and Speth (1995). In the area of membrane fabric material, Karwath et al. (2007) applied orthotropic material constitutive equations and conducted tension experiments in order to extract in-plane stiffness parameters of woven membrane materials under variable ratios of in-plane loading, whereas Bridgens and Gosling (2004) presented two methods for fitting the direct stress-strain representation of coated woven fabrics under biaxial tension. In the area of airbeams, Topping (1963) and Douglas (1969) studied the static response under bending loads, whereas the problem of wrinkling was initially studied by Comer and Levy (1962), Webber (1982) and Main et al. (1994). Veldman et al. (2005) predicted and measured the effect of internal pressure on the deflection of cantilever airbeams. Various authors developed finite elements for predicting the static response of inflated membrane structures (Oden and Sato 1967; Kyriakou et al. 1996). Wielgosz and Thomas (2003) developed a Timoshenko beam finite element and predicted deflections along the span and wrinkling loads of inflatable fabric beams at high internal air pressure subjected to 3-point bending. Reese et al. (2001) applied a hyperelastic material model for the fabric and developed a brick finite element for the coating and non-linear truss elements for the fibers to predict the static response of a membrane under pressure. Cavallaro et al. (2003) developed unit cell models accounting for friction between crossing tows and studied the effect of material, air pressure and loading rate on the mid-span deflection in airbeams subjected to 4-point bending. As far as the dynamic response of membranes is concerned, Jenkins and Korde (2006) published a related state of the art review. Concerning the Tensairity technology, Luchsinger and Crettol (2006) experimentally and numerically studied the static response of Tensairity beams subjected to 3-point bending. The struts, supported by the pneumatic hull, were regarded as beams on an elastic foundation, whose modulus depends on the internal air pressure. Unfortunately, only very few experimental and numerical results (Diaby et al. 2004; Plagianakos et al. 2009) are available for inflated membrane structures subjected to axial compressive loading. Corresponding results would allow assessing the potential of such structural elements for their use as poles in temporary structures.

The application of a fabric web inside the hull, prestressed by the air pressure and supporting the struts along their length, leads to a significant increase in the modulus of the elastic foundation and thus to a stability enhancement. Fabric webs were previously applied by Breuer et al. (2007) to improve the bending

stiffness of Tensairity wing structures. In the current paper, the effect of webs on the static response of a spindle-shaped Tensairity column subjected to axial compressive loading is studied. Two full-scale spindle-shaped columns, one without (plain-spindle) and one with webs (web-spindle), were fabricated and tested for various internal air pressure levels using the experimental configuration described in section 2. An analytical model based on the theory of beams on elastic foundation is presented in section 3. Finite element models of both columns, outlined in section 4, were developed in a commercial finite element code (ANSYS Inc 2007) taking into account linear elastic orthotropic material properties and geometrical non-linearity. In section 5 the response of both columns is compared and evaluated in terms of axial stiffness and buckling load. The effect of internal air pressure on the response of both columns is studied. Moreover, measured and predicted results are compared to indicate the effect of fabrication imperfections on the response. Section 6 summarizes the main observations of the study and indicates possible research extensions.

**Experimental Configuration**

The geometrical characteristics of the two Tensairity columns are shown in Figs. 2(a)-(c). The columns had a span of 5 m and a slenderness of approximately 10. In both columns three circularly arched struts were placed at respective angles of 120° along the section (Fig. 2(b)) and were connected at both ends with cylindrical end parts (Fig. 2(c)). This means that the struts of both columns were in the same position. Each strut was made of aluminum, had a rectangular cross section (30x10 $mm^2$) and was placed in pockets sewed upon the hull. The two cylindrical end parts were also made of aluminum. The hulls, including the webs, were fabricated using a PVC coated polyester fabric material (VALMEX 7318) with a thickness of 0.85 mm. The three webs inside the web-spindle hull ran in the longitudinal direction of the column and supported and interconnected the struts. The angle $\varphi$ (Fig. 2(b)) between hull and struts was determined such as to equally prestress the webs along the span of the column, ranging from 10° in the middle of the column to 35° at the end of the hull. The warp direction of the fabric was in the longitudinal direction of the spindle both for the hull and the webs. After fabrication the maximum radius $R$ of the plain-spindle and the distance $h$ of the web-spindle at mid-span (Fig. 2(b)) were equal to 273 and 250 mm, respectively. The total mass of the web-spindle column (25.1 kg) was 33 % higher than that of the plain-spindle (18.8 kg). As the mass of the three struts plus end pieces was equal to 12.5 kg, the introduction of the webs roughly doubled the mass of the fabric parts.

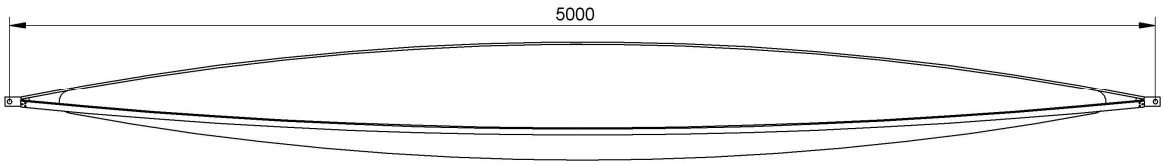


**(a)**

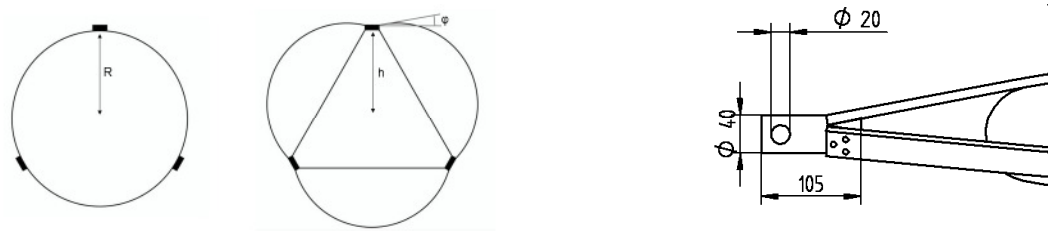


**(b)** **(c)**

**Figure 2** Spindle-shaped columns studied: a) Front view, b) Mid cross-sections of plain-spindle (left) and web-spindle (right), c) Cylindrical end part

**(a)**

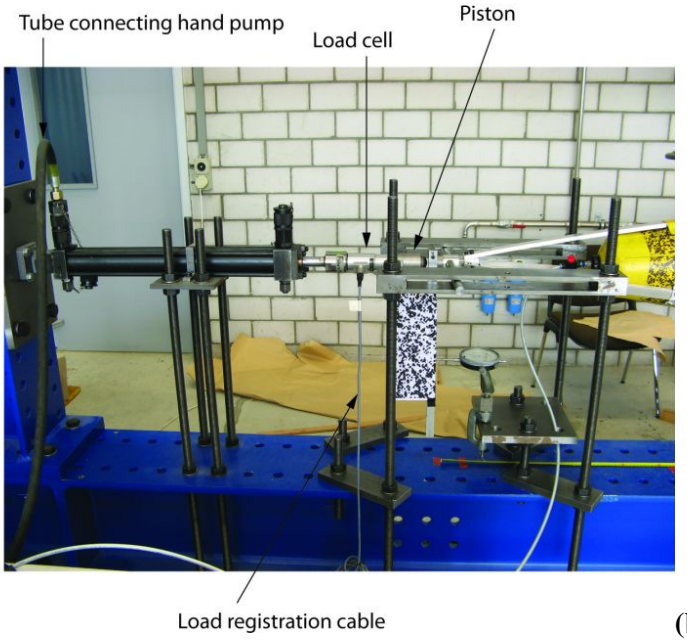


**(b)**

**Figure 3** Experimental configuration for full-scale testing of Tensairity columns subjected to axial compression: a) Overview, b) Load application

The experimental configuration is shown in Figs. 3(a)-(b). The columns were tested in a steel frame under simply-supported boundary conditions. The load was applied at the tip of the column by a hydraulic

piston having a calibrated load cell attached. For every experiment the columns were initially inflated and then subjected to three loading-unloading cycles with a maximum compressive load of 6 kN, in order to minimize the effect of hysteretic behavior (Plagianakos et al. 2009) on the response, and then loaded again until buckling. The axial displacement at the tip and the lateral displacement at various positions along the span were recorded by using dial gauges. The internal air pressure was measured with a digital pressure sensor. The experiments were performed for four different hull pressures: 20, 50, 150 and 250 mbar. The buckled struts were replaced by new ones after every experiment.

**Analytical Model**

In order to develop a simple analytical model for the spindle-shaped Tensairity column, the inflated hull is considered as an elastic foundation for the arched compression struts. Such a model was presented by Plagianakos et al. (2009) based on a flat circular arch approximation. Here, the arch is approximated by a parabola, which allows for simpler analytical expressions. The central assumption of the model is that all three compression elements of the column have an identical behavior. Therefore, only one compression element needs to be modeled.

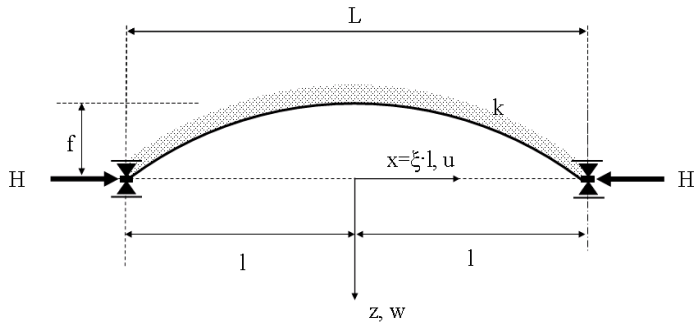


**Figure 4** Basic configuration of the parabolic arch on an elastic foundation model

***Parabolic Arch on Elastic Foundation***

Using the coordinate system and configuration defined in Fig. 4, the shape of a parabolic arch is given by

$$z = -f \cdot \left(1 - \left(\frac{x}{l}\right)^2\right) \tag{1}$$

where $f$ = rise of the arch and $l$ = half span of the column. The lateral displacement $w$ of the elastically embedded arch subjected to a horizontal (axial) load $H$ is given by

$$E \cdot I \cdot \frac{d^4 w}{dx^4} + \frac{d^2 (z + w) \cdot H}{dx^2} + k \cdot w = 0 \tag{2}$$

where $E \cdot I$ = bending stiffness of the compression element and $k$ = modulus of the elastic foundation.

Introducing the dimensionless parameter $\xi$ defined as $x = \xi \cdot l$ with $0 \le \xi \le 1$, one finds from Eq. 1

$$z' := \frac{dz}{d\xi} = l \cdot \frac{dz}{dx} = 2 \cdot f \cdot \xi \tag{3}$$

$$z'' = 2 \cdot f \tag{4}$$

Thus, Eq. 2 can be written in the form

$$w'''' + 8 \cdot \eta \cdot w'' + 16 \cdot \zeta^2 \cdot w = -\frac{2 \cdot f \cdot l^2 \cdot H}{E \cdot I} \tag{5}$$

with

$$\eta = \frac{H \cdot l^2}{8 \cdot E \cdot I}, \quad \zeta = \frac{1}{4} \cdot \sqrt{\frac{k \cdot l^4}{E \cdot I}} \tag{6}$$

Assuming symmetry, $w(\xi) = w(-\xi)$, the general solution of Eq. 5 is given by

$$w(\xi) = C_0 + C_1 \cdot \cos(2 \cdot \lambda_1 \cdot \xi) \cdot \cosh(2 \cdot \lambda_2 \cdot \xi) + C_2 \cdot \sin(2 \cdot \lambda_1 \cdot \xi) \cdot \sinh(2 \cdot \lambda_2 \cdot \xi) \tag{7}$$

with

$$\lambda_1 = \sqrt{\frac{\zeta + \eta}{2}}, \quad \lambda_2 = \sqrt{\frac{\zeta - \eta}{2}} \tag{8}$$

The constant $C_0$ is the particular solution of the inhomogeneous differential equation (5) and $C_1$ and $C_2$ are determined by the two boundary conditions $w(1) = 0$ and $w'(1) = 0$ as described by Plagianakos et al. (2009). One finds

$$C_0 = -\frac{2 \cdot H \cdot f}{k \cdot l^2}$$

$$C_1 = -C_0 \cdot \frac{\lambda_1 \cdot \cos(2 \cdot \lambda_1) \cdot \sinh(2 \cdot \lambda_2) + \lambda_2 \cdot \sin(2 \cdot \lambda_1) \cdot \cosh(2 \cdot \lambda_2)}{\lambda_1 \cdot \sinh(2 \cdot \lambda_2) \cdot \cosh(2 \cdot \lambda_2) + \lambda_2 \cdot \sin(2 \cdot \lambda_1) \cdot \cos(2 \cdot \lambda_1)} \tag{9}$$

$$C_2 = -C_0 \cdot \frac{\lambda_1 \cdot \sin(2 \cdot \lambda_1) \cdot \cosh(2 \cdot \lambda_2) - \lambda_2 \cdot \cos(2 \cdot \lambda_1) \cdot \sinh(2 \cdot \lambda_2)}{\lambda_1 \cdot \sinh(2 \cdot \lambda_2) \cdot \cosh(2 \cdot \lambda_2) + \lambda_2 \cdot \sin(2 \cdot \lambda_1) \cdot \cos(2 \cdot \lambda_1)}$$

The total axial displacement connected with the lateral displacement is given by

$$u = \int_{-l}^{l} dx \cdot \frac{dz}{dx} \cdot \frac{dw}{dx} = \frac{1}{l} \int_{-1}^{1} d\xi \cdot z' \cdot w' = \frac{1}{l} \cdot z' \cdot w \Big|_{-1}^{+1} - \frac{1}{l} \int_{-1}^{1} d\xi \cdot z'' \cdot w = -\frac{4 \cdot f}{l} \int_{0}^{1} d\xi \cdot w \tag{10}$$

By using Eq. 7, the integral can be evaluated and one finds

$$u = -\frac{4 \cdot f}{l} \cdot C_0 - \frac{4 \cdot f}{l} \cdot \left[ \cos(2 \cdot \lambda_1) \cdot \sinh(2 \cdot \lambda_2) \cdot \left( \frac{C_1 \cdot \lambda_2 - C_2 \cdot \lambda_1}{2 \cdot \lambda_1^{\,2} + 2 \cdot \lambda_2^{\,2}} \right) + \sin(2 \cdot \lambda_1) \cdot \cosh(2 \cdot \lambda_2) \cdot \left( \frac{C_1 \cdot \lambda_1 + C_2 \cdot \lambda_2}{2 \cdot \lambda_1^{\,2} + 2 \cdot \lambda_2^{\,2}} \right) \right] \tag{11}$$

Simple approximations for the analytical lateral and axial displacement can be given for the problem at hand. The lateral displacement at midspan ( $\xi = 0$ ) is given by (Eq. 7)

$$w(0) = C_0 + C_1 \tag{12}$$

The first term in this equation is much larger than the second one for the given column; e.g., the ratio $C_1 / C_0$ decreases from 0.02 for $p = 20$ mbar to 0.0004 for $p = 250$ mbar in the case of the plain-spindle. Therefore, we can approximate the lateral displacement at midspan by

$$w(0) \approx C_0 = -\frac{2 \cdot H \cdot f}{k \cdot l^2} \tag{13}$$

A simple approximation can also be found for the axial displacement *u*. One can show that, for the column at hand, the two terms with trigonometric and hyperbolic functions in Eq. 11 are small compared to the first term. Thus,

$$u \approx -\frac{4 \cdot f}{l} \cdot C_0 = \frac{8 \cdot H \cdot f^{\,2}}{k \cdot l^3} = \frac{8 \cdot P_{tot}}{3 \cdot k \cdot l \cdot \gamma^2} \tag{14}$$

where the slenderness $\gamma = 2 \cdot l / (2 \cdot f)$ has been introduced. The total applied axial load $P_{tot}$ is equally distributed over the three compression elements and thus

$$H = P_{tot} / 3 \tag{15}$$

The axial displacement of the compression strut due to elasticity of the material is given by

$$u_{el} = \frac{P_{tot} \cdot 2 \cdot l}{3 \cdot E \cdot A} \tag{16}$$

with $A$ = the cross-sectional area of a single compression element. As shown by Plagianakos et al. (2009), this is a significant contribution to the total axial displacement and cannot be neglected.

The axial stiffness of the Tensairity column is defined as

$$m = \frac{P_{tot}}{u + u_{el}} \tag{17}$$

By means of Eqs. 14-16, one obtains

$$m = \frac{3}{8} \cdot k \cdot l \cdot \gamma^2 \cdot \frac{1}{1 + \frac{k \cdot l^2 \cdot \gamma^2}{4 \cdot E \cdot A}} \tag{18}$$

which is a simple analytical approximation for the axial stiffness of the Tensairity column. The axial stiffness depends on the slenderness, the span, the modulus of the foundation as well as on the Young's modulus and cross-sectional area of the compression strut. The axial stiffnesses of the plain-spindle and the web-spindle only vary due to the different modulus of the elastic foundation of these two Tensairity structures.

***Plain-spindle***

The modulus of the elastic foundation for the plain-spindle is a function of the air pressure. For three compression elements, it is given by (Plagianakos et al. 2009)

$$k_{plain} = \pi \cdot p \cdot \frac{2 \cdot \sqrt{3}}{3 \cdot \sqrt{3 - \pi}} \tag{19}$$

The lateral displacement of the plain-spindle (Eqs. 7 and 9) for a total applied load of 3 kN is shown for four pressure values in Fig. 5. The cross-section of the aluminum struts is defined above and the elastic properties are given in Table 1; furthermore $f$ = 273 mm and $l$ = 2500 mm. The displacement is rather constant in the central region of the spindle and drops to zero at the ends as enforced by the boundary conditions.

The calculated axial stiffness for the column for four pressure values is given in Table 2. The approximation $m_{approx}^{par}$ as defined by Eq. 18 as well as the exact result $m_{exact}^{par}$ (Eqs. 11 and 17) are given in the first and second column of the table. In the last column, the axial stiffness from the model based on circular arches $m_{exact}^{circle}$ (Plagianakos et al. 2009) is given for comparison. The applied total load was equal to 3 kN. The approximated axial stiffness is lower than the exact stiffness for all pressure values and thus the stiffness is underestimated by the approximation. The difference ranges from 15 % (20 mbar) to 5 % (250 mbar). The difference in the stiffness between the model based on a parabola as presented here and the model based on circular arches is less than 2 %. Therefore, both models lead to very similar results.

| **Material** | Aluminum | Fabric |
|---|---|---|
| *Elastic Properties* | | |
| $E_{11}$ (GPa) | 68.0 | 0.820 |
| $E_{22}$ (GPa) | 68.0 | 0.635 |
| $G_{12}$ (GPa) | 26.2 | 0.014 |
| $v_{12}$ | 0.30 | 0.23 |

**Table 1** In-plane elastic properties of considered materials

| Pressure [mbar] | $m_{approx}^{par}$ [kN/mm] | $m_{exact}^{par}$ [kN/mm] | $m_{exact}^{circle}$ [kN/mm] |
|---|---|---|---|
| 20 | 0.784 | 0.922 | 0.945 |
| 50 | 1.79 | 2.03 | 2.04 |
| 150 | 4.15 | 4.48 | 4.44 |
| 250 | 5.64 | 5.97 | 5.89 |

**Table 2** Analytically predicted axial stiffnesses for the plain-spindle

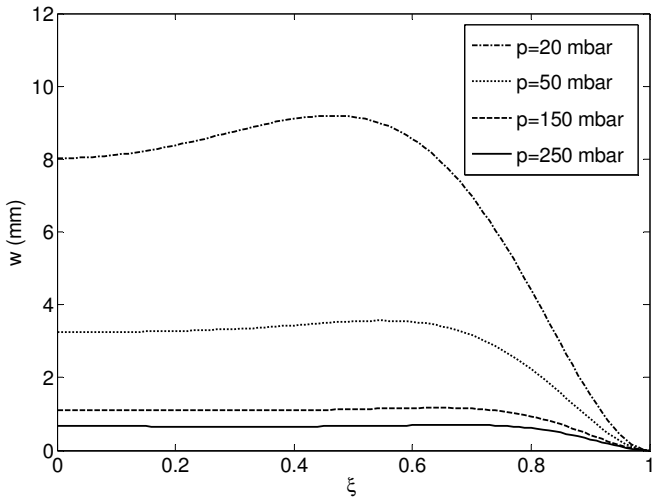


**Figure 5** Calculated lateral displacement of the plain-spindle for a total axial load of 3 kN

***Web-spindle***

The modulus of the elastic foundation for the web-spindle is determined by the elastic properties of the webs. Obviously, the fabric web can resist outward lateral forces leading to an increased tensioning of the web. Since the webs are prestressed due to the internal pressure, they can also resist inward compressive forces up to the prestressing. For a triangular web configuration as presented in Fig. 2(b), the modulus of the elastic foundation is given by

$$k_{web} = \frac{\sqrt{3} \cdot E^{l}_{web} \cdot t}{h} \tag{20}$$

where $E^{l}_{web}$ = Young's modulus of the web in the lateral direction and $t$ = thickness of the web (0.85 mm). The same fabric was used for the web and the hull. The lateral direction of the web corresponds to the fill direction of the fabric in the design of the web-spindle and thus $E^{l}_{web} = E_{22}$ as given in Table 1. The parameter $h$ is the distance from the symmetry axis of the column to the compression element which corresponds to 250 mm at midspan. The modulus of the foundation at the center of the web-spindle is $k_{web}$ = 3.74 MPa while the modulus of the foundation for the plain-spindle for a pressure of 250 mbar is $k_{plain}$ = 0.13 MPa. Thus, by introducing the web, the modulus of the foundation can be increased by almost a factor of 30. Or, to put it differently, an air pressure of 7 bar would be needed to achieve the same modulus of the foundation for a plain-spindle as for the given web-spindle, leading to an enormous hoop stress which cannot be taken up by the fabrics typically used in civil engineering applications.

As $h$ is not constant along the length of the column and decreases towards the ends, the modulus of the foundation becomes a function of the position along the column in the case of a web-spindle. Thus, the analytical solution (Eq. 7) will not be valid in this case and Eq. 2 needs to be solved numerically. However, in order to obtain a first guess for the axial stiffness of the web-spindle, the axial stiffness (Eq. 18) for the web-spindle with constant modulus of the foundation equals 11.7 kN/mm, which is very close to the elastic limit $3EA/(2l)$ of the compression elements (12.2 kN/mm). Obviously, the stiffness is (in the model) independent of the air pressure, since the modulus of the foundation does not depend on the pressure. The exact numerical treatment of Eq. 2 with position dependent modulus of the foundation will lead to an even higher axial stiffness, as the modulus increases towards the ends of the column. However, since the elastic limit of the compression element is in any case the upper bound, the increase of the stiffness due to the exact numerical solution is not large and was calculated to be only 1 %. Based on these considerations one can expect a very high axial stiffness for the web-spindle due to a highly increased modulus of the foundation.

Eq. 18 reveals that the axial stiffness of the Tensairity column does not depend on the bending stiffness $E \cdot I$ of the compression element within this approximation. However, the axial stiffness strongly depends on the slenderness of the column. The axial stiffness (Eq. 18) as a function of slenderness is shown for four pressure values of the plain-spindle as well as for the web-spindle in Fig. 6. The slenderness of the

given columns is around 10. For higher slenderness values and a higher modulus of the elastic foundation, the axial stiffness eventually reaches the limit of the material elasticity (Eq. 17). For the web-spindle this limit is almost reached for a slenderness of 10.

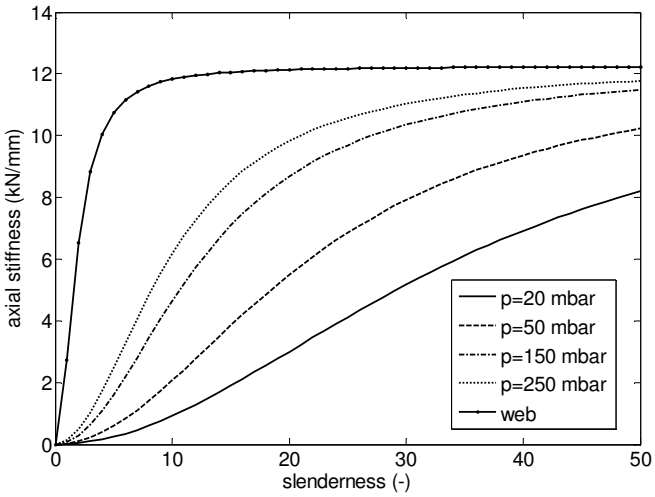


**Figure 6** Calculated axial stiffness of the plain-spindle with four different pressure values and for the web-spindle as a function of the slenderness

**Finite Element Models**

The finite element models developed in ANSYS are shown in Figs. 7(a)-(b) and 8(a)-(c) for the plain-spindle and web-spindle, respectively. The fabric hull and the webs were modeled by four-node shell elements (SHELL 181) whose bending stiffness was not taken into account in the solution by means of a feature provided in the element properties. The plain-spindle was exclusively modeled in ANSYS and two-node Timoshenko beam elements (BEAM 188) were used to model the struts. On the other hand, the geometry of the web-spindle was imported from a CAD software and took into account voids between the hull's circular sections (Fig. 2(b)). Thus, four-node shell elements (SHELL 181) were applied in the case of the web-spindle struts for the parts of the struts supported by the hull and two-node Timoshenko beam elements (BEAM 188) for the parts outside the hull. A non-uniform mesh was applied for both hulls and the webs, being finer near the ends of the columns. A tight connection between hull and struts was assumed in all cases studied. The woven fabric material was modeled as a UD ply with linear orthotropic properties representing mean values of biaxial testing measurements conducted on specimens of the same fabric (Galliot and Luchsinger 2009). The material properties for both fabric and struts are listed in Table 1. Both Tensairity columns had a span defined as the distance between the rotation points of the end pieces, whereas the end

pieces were not modeled. Simply-supported boundary conditions were considered in both spindle cases studied (Figs. 7(a) and 8(a)).

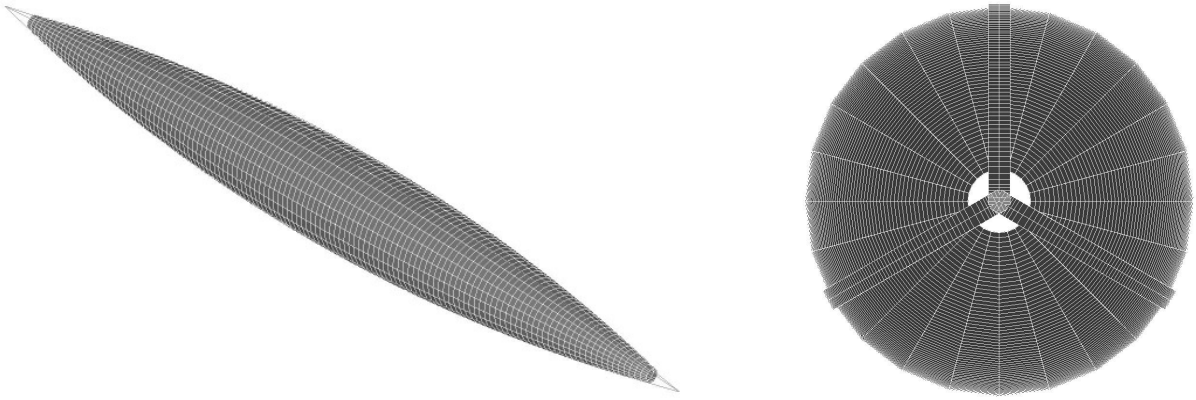

**(a)** **(b)**

**Figure 7** FE model of the plain-spindle: a) Isometric view, b) Side view

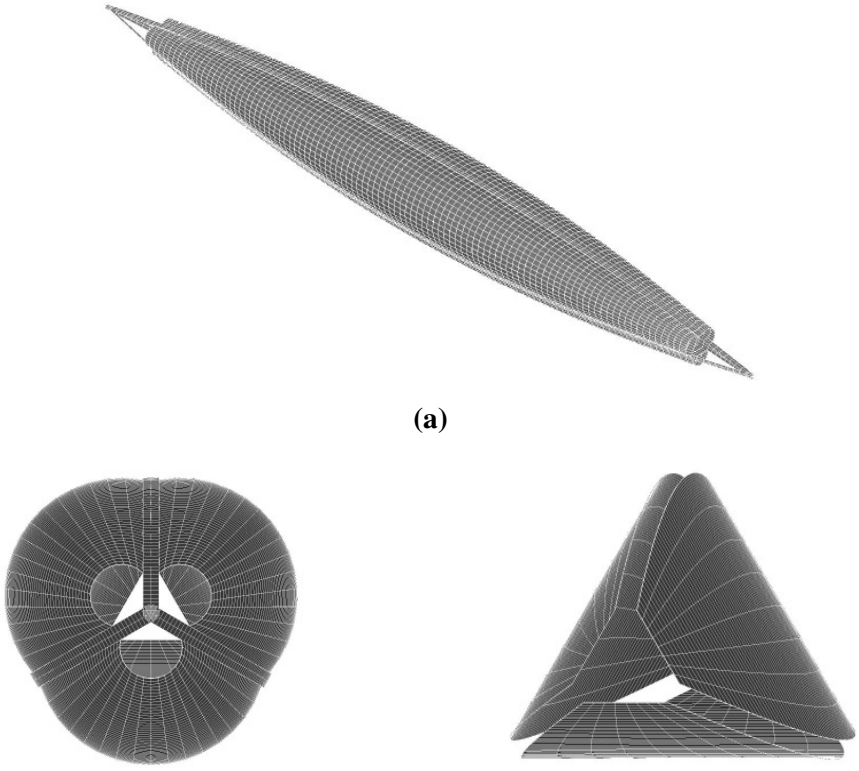

**(a)**

**(b)** **(c)**

**Figure 8** FE model of the web-spindle: a) Isometric view, b) Side view, c) Fabric webs

The geometrically non-linear solution took place in two successive steps: 1) inflation and 2) axial compressive loading. At inflation outward pressure loading was applied on the surface of the hull elements and additionally, in the case of the web-spindle, on the bottom of the struts. No pressure was applied on the fabric webs, since they undergo pressure loading on both sides which is equal in size and opposite in direction. The forces of the air pressure were always kept normal to the surface during the displacements

under inflation. The inflation was done in 10 substeps for each pressure level. The compressive load was applied in substeps of 0.25 kN in the plain-spindle case, whereas the size of the substeps varied in the web-spindle case, being in the range between 0.25 kN and 0.5 kN. The buckling load was determined with respect to the last convergent substep of the solution and by inspection of the corresponding buckling mode shape.

**Results and Discussion**

A typical measurement of the axial displacement at the tip of the plain-spindle column for an internal pressure value of $p$ = 250 mbar is shown in Fig. 9. Similar load-displacement curves were acquired for both plain- and web-spindle for all internal air pressure levels studied. The measured non-linear response can be partitioned in four phases, as shown in Fig. 9, indicating different axial stiffness values of the column. The second phase, indicated as main compressive phase, illustrates a range of applicability of a Tensairity column under axial compressive loading in practical cases and yields a nearly constant slope, which indicates the axial stiffness of the column under compressive loading.

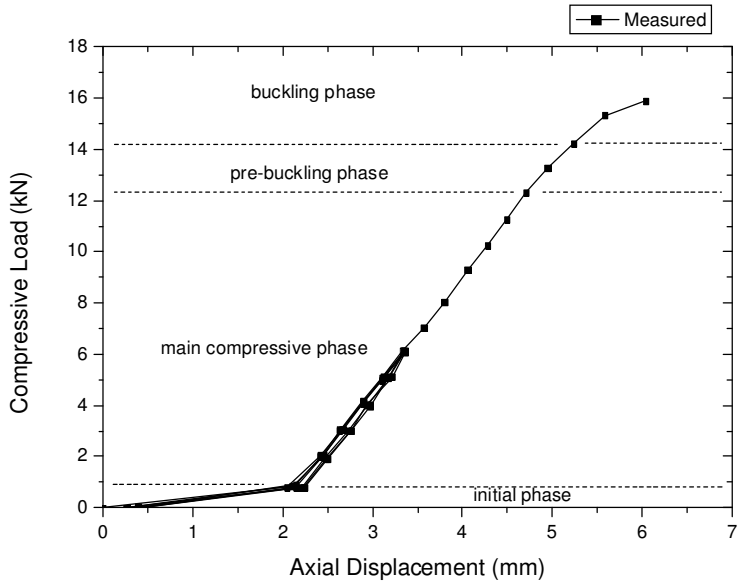


**Figure 9** Load-axial displacement curve of the plain-spindle column for an internal air pressure of $p$ = 250 mbar

The effect of internal air pressure on the measured response at the tip of the plain-spindle and web-spindle is illustrated in Figs. 10(a)-(b), respectively. In both cases an increased hull pressure improves the stiffness and load bearing capacity of the column; however, the effect of pressure is more pronounced for the plain-spindle.

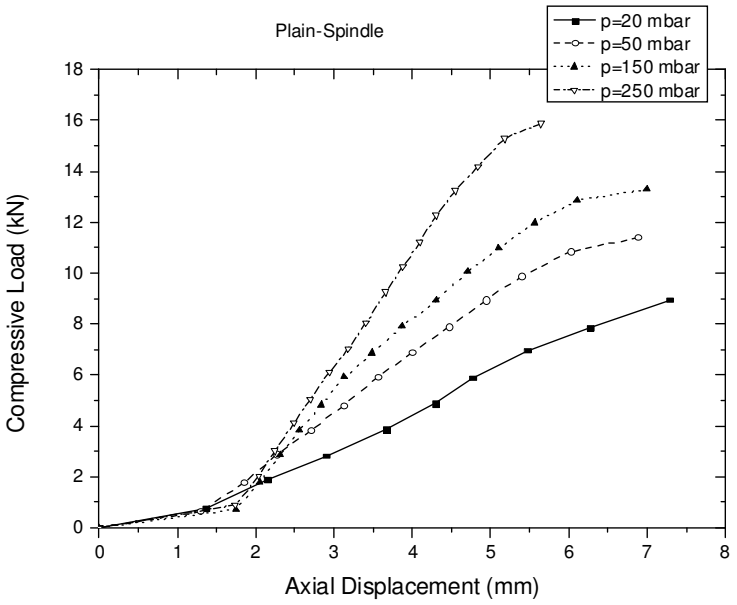


**(a)**

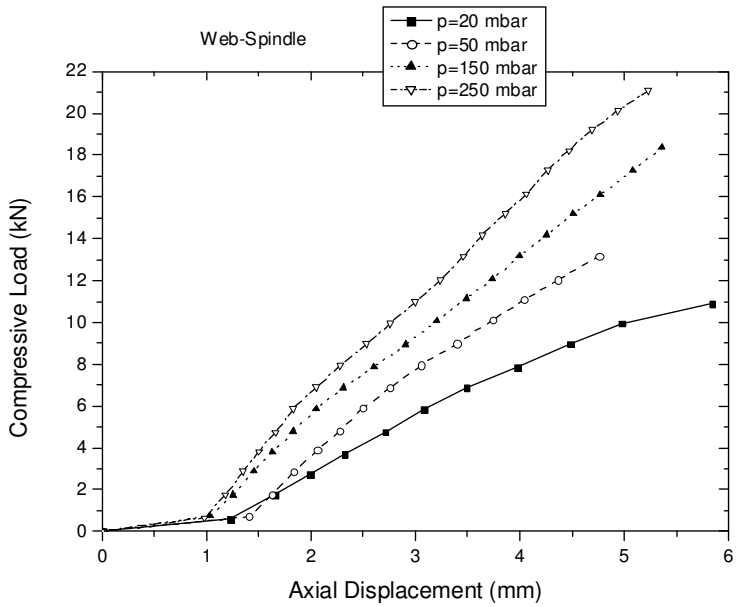


**(b)**

**Figure 10** Effect of internal air pressure on the measured load-axial displacement curves for the loading semi-cycle up to buckling: a) Plain-spindle, b) Web-spindle

Comparison of the load-displacement curves of the plain- and web-spindle reveals that the addition of the fabric webs clearly improves the axial stiffness of the column. This is highlighted in Fig. 11, which shows the slopes of the experimental as well as the predicted load-axial displacement curves for both columns at various air pressure levels. The slope is determined between 1 and 6 kN in the loading semi-cycle up to buckling. The measured improvement in stiffness is a factor 2 for lower pressures and slightly less for higher pressure levels. The analytical predictions (Eq. 18) and FE predictions show a larger improvement of

the axial stiffness by the application of webs. Whereas the predicted results for the plain-spindle correlate well with the experimental ones, the deviation between both is larger for the web-spindle, which is ascribed to a lower effective stiffness of the webs in practice. Besides, the axial stiffness of the response of the web-spindle appears to be independent of the hull pressure for both the analytical and FE predictions, which is due to the linear-elastic fabric webs providing the lateral support of the struts. The fact that these predictions are not far off the theoretical axial stiffness of the struts (Eq. 16) illustrates the effectiveness of the supporting webs in an ideal situation. Finally, the good resemblance of the analytical and FE predictions in Fig. 11 validates the simplified analytical model.

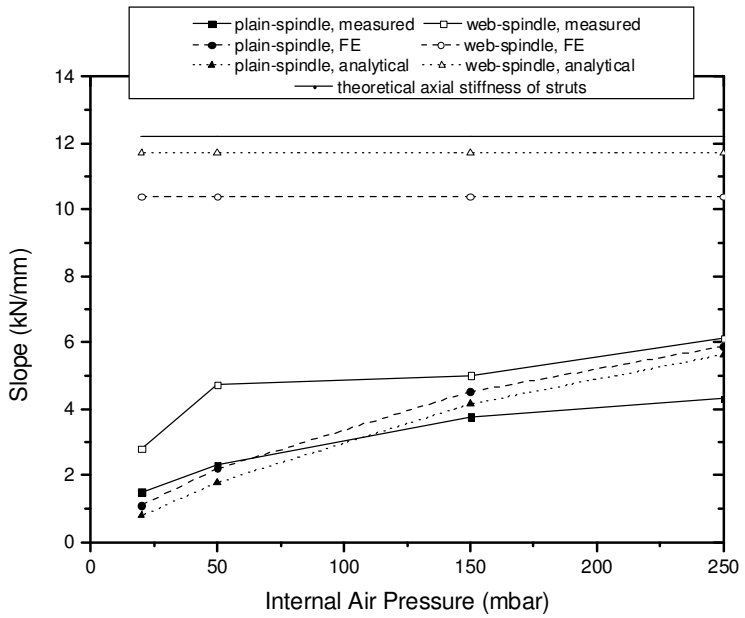


**Figure 11** Effect of internal air pressure on the analytical, numerical and experimental slopes of the load-axial displacement curves of the columns

Fig. 12 shows the experimental and numerical buckling loads for both columns at various internal air pressure levels. Both approaches show an increase of the buckling load by the application of webs. In case of the experiments the relative increment is larger for higher pressure levels, approaching a 40 % improvement for 150 mbar. Regarding the FE results the buckling load of the web-spindle is twice as large for 20 mbar and gradually decreases for higher pressure levels. The buckling loads of both FE models increase with air pressure, although the web-spindle is rather insensitive due to the pressure-independent stiffness of the supporting and interconnecting webs. The predicted load bearing capacities are considerably larger than the measured ones, which is attributed to imperfections in the experimental models due to fabrication. In case of the web-spindle the lower effective stiffness of the webs also has an effect.

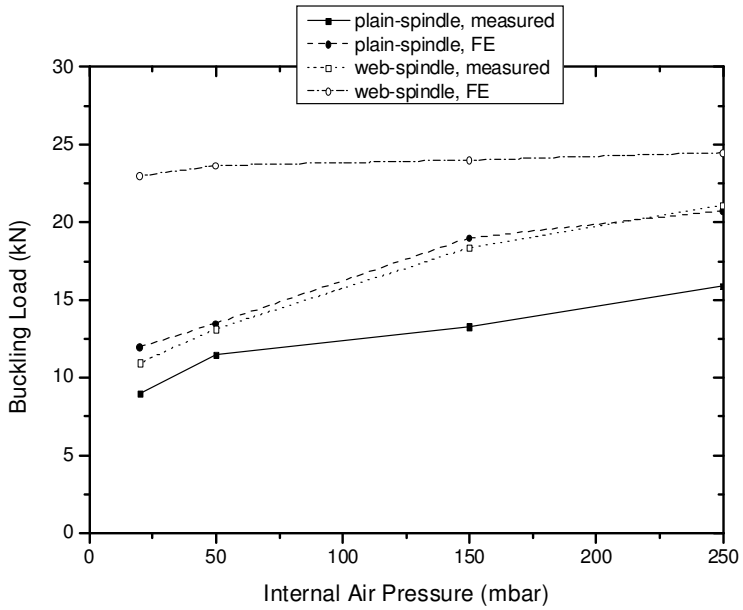


**Figure 12** Effect of internal air pressure on the analytical, numerical and experimental buckling loads of the columns

The deviations between the experimental and predicted axial stiffness of the web-spindle were ascribed to a lower effective stiffness of the webs in practice. One of the explanations for this behavior is the connection between the strut and the web in the fabricated model. In practice the web is not directly connected to the strut, but to the pocket. A lateral displacement of the strut under loading is therefore transferred to the webs through the pocket, thus lowering the stiffness of the elastic foundation and therefore the axial stiffness of the column. The effect of this indirect connection increases when the pocket welds show signs of deterioration (peeling) during the last experiments. To gain better insight, the lateral displacement of the web-spindle was measured during inflation. It was found to be about 8 mm at midspan for a pressure of 250 mbar and thus much larger than the 0.6 mm predicted from the analytical model. Thus, the modulus of the elastic foundation of the web-spindle (Eq. 20) must be much smaller in reality. In fact, the web's Young's modulus has to be reduced by a factor of 15 in order to predict the measured lateral displacement during inflation. With such a small effective Young's modulus for the web, the FE predictions for the axial stiffness range from 8.16 to 8.31 kN/mm depending on the hull pressure. Therefore, at least part of the deviation between prediction and measurement can be attributed to a large overestimation of the stabilization effect of the web in the ideal configuration of the analytical and numerical model.

Besides the hull-strut connection also imperfections due to fabrication are ascribed a reducing effect on the stiffness of the strut's lateral support. The web-spindle has to be fabricated with tolerances less than a

millimeter in order to acquire an evenly prestressed web over its length. Unfortunately, this level of accuracy is almost impossible to reach in the manufacturing of fabric structures, leading to further deviations between the measured and the predicted values.

## Conclusions

Experiments on spindle-shaped Tensairity columns have demonstrated the stiffening and stabilizing effect of the air pressure in this new structural concept. Both axial stiffness and load bearing capacity increase with hull pressure. Furthermore, the application of fabric webs inside the hull leads to an improvement of the structural behavior of the column, which is confirmed by the analytical and numerical predictions. For all regarded pressures both axial stiffness and buckling load clearly increase due to the webs. The improved structural behavior can be ascribed to the additional support provided by the webs and the better cooperation between the struts due to the interconnecting webs. In general there is a sound correlation between the analytical, numerical and experimental results for the plain-spindle. However, in case of the web-spindle, the theory based on an ideal web-spindle predicts a significantly higher axial stiffness than measured. The effective stiffness of the webs appears to be lower in practice than expected, which is ascribed to geometrical imperfections in the webs and the indirect connection between strut and webs of the actual structure. Consequently, a considerable improvement is expected to be gained by an improved design and fabrication of the web-spindle. Future studies will focus on such improvements. Furthermore, full-scale testing of Tensairity structures with fabric webs subjected to bending will provide deeper insights in the advantages of applying webs in Tensairity structures.

## Acknowledgements

The authors would like to thank HP Gasser AG for the fabrication of the hulls. The financial support of Festo is also gratefully acknowledged.

**Notation**

*The following symbols are used in the paper:*

$x$ = axial coordinate;

$z$ = lateral coordinate;

$u$ = axial displacement;

$w$ = lateral displacement;

$f$ = rise of arch;

$l$ = half span of column;

$L$ = span of column;

$h$ = distance between strut and symmetry axis of column;

$R$ = radius of the hull of the plain-spindle;

$t$ = thickness of the hull;

$A$ = cross-sectional area of compression element;

$\varphi$ = angle between hull and compression element;

$\gamma$ = slenderness of the column;

$p$ = air pressure;

$k$ = modulus of elastic foundation;

$m$ = axial stiffness;

$H$ = axial load on a single strut;

$P_{tot}$ = total axial load on the column;

$E$ = Young's modulus;

$I$ = moment of inertia of the compression element;

$C_0$ ,$C_1$, $C_2$ = integration constants;

$\xi$ = dimensionless coordinate;

$\lambda_1$, $\lambda_2$ = length-scale parameters;

$\zeta$, $\eta$ = abbreviation parameters.

**References**


ANSYS Inc (2007). *ANSYS Users Manual for ANSYS Rev. 11.0*, Canonsburg (PA).

Bernasconi, M.C., and Reibaldi, C.G. (1986). "Inflatable space-rigidized structures: Overview of applications and their technology impact." *Acta Astronautica*, 14, 455-465.

Bird, W.W. (1967). "The development of pneumatic structures: Past, present, future." *1st International Colloquium on Pneumatic Structures*, Technische Hochschule Stuttgart.

Breuer, J., Ockels, W., and Luchsinger, R.H. (2007). "An inflatable wing using the principle of Tensairity." *Proc. AIAA Conference*, Hawaii.

Bridgens, B.N., and Gosling, P.D. (2004). "Direct stress-strain representation for coated woven fabrics." *Computers & Structures*, 82(23-26), 1913-1927

Bulson, P.S. (1973). "Design principles of pneumatic structures." *The Structural Engineer*, 51, 209-215.

Cavallaro, P.V., Johnson, M.E., and Sadegh, A.M. (2003). "Mechanics of plain-woven fabrics for inflated structures." *Composite Structures*, 61(4), 375-393.

Comer, R.L., and Levy, S. (1962). "Deflections of an inflated circular-cylindrical cantilever beam." *AIAA Journal*, 1(7), 1652-1655.

Diaby, A., Wielgosz, C., Le Van, A. (2004). "Buckling force of inflated tubes under axial compression: Numerical computations versus experiments." *Proc. IASS Symposium*, Montpellier.

Douglas, W.J. (1969). "Bending stiffness of an inflated cylindrical cantilever beam." *AIAA Journal*, 7(7), 1248-1253.

Galliot, C., Luchsinger, R.H. "A simple model describing the non-linear biaxial tensile behaviour of PVC-coated polyester fabrics for use in finite element analysis." Under review in *Composite Structures*.

Herzog, T. (1976). *Pneumatische Konstruktionen*, Gerd Hatje Verlag, Stuttgart.

Jenkins, C.H.M., and Korde, U.A. (2006). "Membrane vibration experiments: An historical review and recent results." *Journal of Sound and Vibration*, 295(3-5), 602-613.

Karwath, M., Wagner, R., and Kroeplin, B. (2007). "Ein orthotropes Werkstoffgesetz für Folien." *Stahlbau*, 76(5), 297-304.

Kyriakou, S.K., Schwab, C., and Humphrey, J.D. (1996). "Finite element analysis of nonlinear orthotropic hyperelastic membranes." *Computational Mechanics*, 18(4), 269-278.

Luchsinger, R.H., Pedretti, A., Steingruber, P., Pedretti, M. (2004). "The new structural concept Tensairity: Basic principles." *Progress in Structural Engineering, Mechanics and Computations*, A.A. Balkema Publishers, London.

Luchsinger, R.H., and Crettol, R. (2006). "Experimental and numerical study of spindle shaped Tensairity girders." *International Journal of Space Structures*, 21(3), 119-130.

Main, J.A., Peterson, S.W., and Strauss, A.M. (1994). "Load-deflection behavior of space-based inflatable fabric beams." *Journal of Aerospace Engineering*, 7(2), 225-238.

Oden, J.T., and Sato, T. (1967). "Finite strains and displacements of elastic membranes by the finite element method." *International Journal of Solids and Structures*, 3(4), 471-488.

Otto, F., and Trostel, R. (1962). *Zugbeanspruchte Konstruktionen – Band 1*, Ullstein Fachverlag, Frankfurt and Berlin.

Plagianakos, T.S., Teutsch, U., Crettol, R., and Luchsinger, R.H. "Static response of a spindle-shaped Tensairity column to axial compression." accepted in *Engineering Structures*.

Reese, S., Raible, T., and Wriggers, P. (2001). "Finite element modeling of orthotropic material behaviour in pneumatic membranes." *International Journal of Solids and Structures*, 38(52), 9525-9544.

Sobek, W., and Speth, M. (1995). "Textile Werkstoffe." *Bauingenieur*, 70, 243-250.

Topping, A.D. (1963). "Shear deflections and buckling characteristics of inflated members." *Journal of Aircraft*, 1(5), 289-292.

Veldman, S.L., Bergsma, O.K., and Beukers, A. (2005). "Bending of anisotropic inflated cylindrical beams." *Thin Wall Structures*, 43(3), 461-475.

Webber, J.P.H. (1982). "Deflections of inflated cylindrical cantilever beams subjected to bending and torsion." *Aeronautical Journal*, 86(10), 306-312.

Wielgosz, C., Thomas, J.C. (2003). "An inflatable fabric beam finite element." *Communications in Numerical Methods in Engineering*, 19(4), 307-312.